frontiers in Earth Science

ORIGINAL RESEARCH
published: 07 December 2021
doi: 10.3389/feart.2021.778025

# Hydrocarbon Potential of the Late Permian and the Late Triassic Source Rocks from the Qamdo (Changdu) Basin, Eastern Tibet and Its Linkage with the Sea Level Change

*Zhaolin Qi*[1,2]*, *Yalin Li*[2]* and *Chengshan Wang*[2]

[1]Department of Geological Engineering, Qinghai University, Xining, China, [2]School of Earth Science and Resources, China University of Geosciences, Beijing, China

The Qamdo Basin in eastern Tibet has significant petroleum potential and previous studies indicate that the basin contains thick potential source rocks of the Late Permian and the Late Triassic ages. In this paper, the petroleum potential of samples from measured the Upper Permian and Upper Triassic outcrop sections were evaluated on the basis of sedimentological, organic petrographic and geochemical analyses. Initial evaluations of total organic carbon contents indicated that shale samples from the Upper Permian Tuoba Formation and the Upper Triassic Adula and Duogala Formations have major source rock potential, while carbonate rocks from the Upper Triassic Bolila Formation are comparatively lean in organic matter More detailed analyses of OM-rich shale samples from the Tuoba, Adula and Duogala Formations included Rock-eval, elemental analyses, gas chromatography and organic petrography. Maceral compositions and plots of atomic O/C versus H/C indicate that the organic matter present in the samples is primarily Type II with a mixed source. Analyses of acyclic isoprenoid biomarkers indicate the organic matter was deposited under reducing and sub-to anoxic conditions. Based on the high vitrinite reflectance (Ro>1.3%) and Rock-eval data, the samples are classified as highly to over-mature, suggesting that the Tuoba, Adula and Duogaila Formation shales may generate thermogenic gas. Source rock intervals in the three formations are interpreted to have been deposited in marginal-marine environment during transgressions and under a warm and moist climatic condition.

**Keywords: Qamdo Basin, eastern Tibet, organic geochemistry, source rock, shale**

OPEN ACCESS

***Edited by:***
*Ziqi Feng,*
*China University of Petroleum, Huadong (UPC), China*

***Reviewed by:***
*Pengfei Ma,*
*Tongji University, China*
*Tian Dong,*
*China University of Geosciences Wuhan, China*

***Correspondence:**
*Zhaolin Qi*
*zhlqi_qhu@163.com*
*Yalin Li*
*liyalin@cugb.edu.cn*

***Specialty section:***
*This article was submitted to Economic Geology, a section of the journal Frontiers in Earth Science*

***Received:*** *16 September 2021*
***Accepted:*** *22 November 2021*
***Published:*** *07 December 2021*

***Citation:***
*Qi Z, Li Y and Wang C (2021) Hydrocarbon Potential of the Late Permian and the Late Triassic Source Rocks from the Qamdo (Changdu) Basin, Eastern Tibet and Its Linkage with the Sea Level Change. Front. Earth Sci. 9:778025. doi: 10.3389/feart.2021.778025*

## INTRODUCTION

Tibet is located in the eastern part of the petroliferous Tethyan realm (Klemme and Ulmishek, 1991). However, compared to analogous areas to the west such as the Persian Gulf and the Caucasus, petroleum exploration in Tibet has not been successful due mainly to the complexity of the tectonic history (Yin and Harrison, 2000; DeCelles et al., 2002; Wang et al., 2014). Nevertheless, oil shows have been recorded in the Qiangtang Basin which is believed to have significant exploration potential (Fu et al., 2009; Yang et al., 2015). Over 200 surface seeps of solid petroleum have been found at

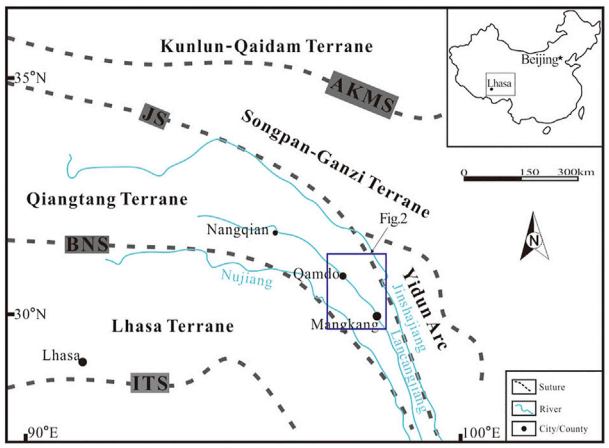


**FIGURE 1 |** Simplified structural map of eastern Tibet showing the major suture zones and rivers (modified from Deng et al., 2014). Abbreviations: AKMS, Anyimaqin-Kunlun-Muztagh suture; JS, Jinshajiang suture; BNS, Bangong-Nujiang suture; ITS, Indus-Tsangpo suture.

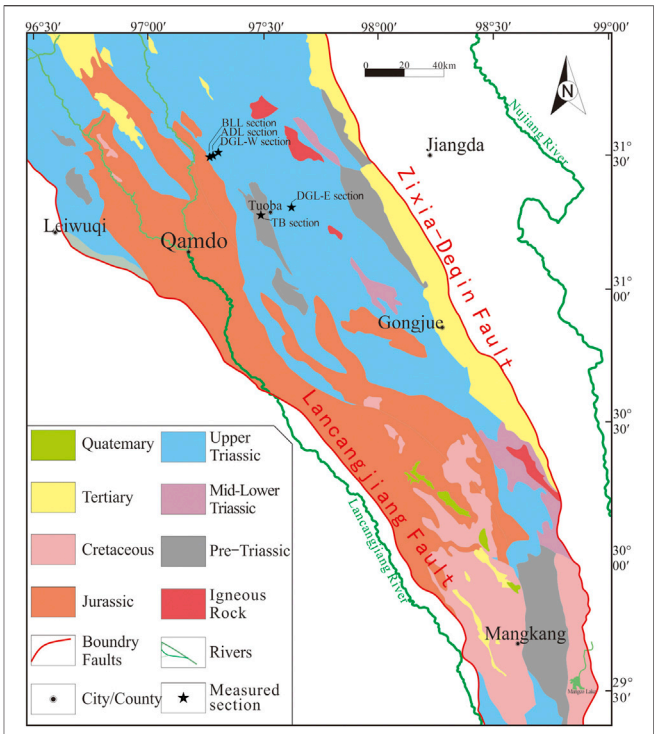


**FIGURE 2 |** Geological map of the Qamdo Basin showing the location of the measured sections (modified form Tibet BGMR [Tibet Bureau of Geology and Mineral Resources], 2007).

outcrop and five potential petroleum systems have been identified within the Mesozoic succession (Tan et al., 2002; Wang et al., 2009; Zeng et al., 2013). In addition, the Tertiary continental basins, such as the Lunpola Basin, have been received attention as they have the most promising source rocks (Wang et al., 2011a). It was reported that the 'industrial" oil flow was discovered at two wells of the Lunpoa Basin in 1990s (Gu et al., 1999). The Tibetan Plateau is therefore considered be an exploration Frontier with numerous under-explored marine and continental petroliferous basins (Taner and Meyerhoff, 1990a; Wang and Zhang, 1996; Wang et al., 2006).

The Qamdo Basin in eastern Tibet covers an area of more than 10,000 km$^2$ and is similar to the Qiangtang Basin in terms of age, stratigraphy and tectonic setting. Preliminary field surveys (Sichuan BGMR [Sichuan Bureau of Geology and Mineral Resources], 2007; Tibet BGMR [Tibet Bureau of Geology and Mineral Resources], 2007) indicate that thick black shales are exposed at outcrop over large areas of the basin and may have significant hydrocarbon potential. Chen et al. (2010) proposed that the paleo-oil reservoirs in Qamdo area charged with four events during foreland basin stage from the early Jurassic to the early Cretaceous, which had been destroyed or cracked during the strike-slip basin stage of the Cenozoic. The presence of oil-saturated sandstones (Xu et al., 2004) and seepages (Taner and Meyerhoff, 1990b) together with evidence from fluid inclusions in Mesozoic reservoir rocks (Chen et al., 2010; Wu et al., 2010) indicate that hydrocarbon generation, migration and accumulation have taken place in the basin. Moreover, previous study (Du et al., 1997; Peng et al., 2005) of the Late Palaeozoic sequence stratigraphy in the Qamdo Basin unveiled the sea level change of the Qamdo block.

However, detailed studies of source rocks and its linkage with the sea level change have not yet been undertaken. In this study, we investigate the Upper Permian and the Upper Triassic organic rich shales at five outcrop locations in the Qamdo Basin. The purpose of the paper is to analyse the samples' sedimentological and organic geochemical characteristics and to evaluate their hydrocarbon potential. Factors controlling source rock deposition including sea level changes, climatic variations and regional tectonics, are briefly reviewed.

## GEOLOGICAL SETTING

The Tibetan Plateau is composed of a series of continental terranes which were accreted to the margin of the Eurasian Plate during the Palaeozoic and Mesozoic (Chang et al., 1986; Yin and Harrison, 2000; Pan et al., 2012). The NW-SE elongated Qamdo Basin in eastern Tibet, the focus of this study, is located on the Precambrian crystalline basement of the Qiangtang-Qamdo terrane (Du et al., 1998). From stratigraphic and structural data, the Qiangtang Terrane can be divided from west to east into the Qiangtang Block in central Tibet and the Qamdo Block to the SE (Chang et al., 1989; Huang et al., 1992), which is sandwiched between the Jinshajiang and Bangong-Nujiang suture zones (**Figure 1**). The former suture marks the boundary between the Yidun Arc complex and the Qiangtang Terrane which formed during closure of the PalaeoTethys, while the latter separates the Lhasa and Qiangtang Terranes which formed during closure of the MesoTethys (Yin and Harrison, 2000).

After the amalgamation of continental blocks and terranes during the Palaeozoic and Mesozoic, regional tectonism during the Cenozoic including the India-Asia collision reshaped the lithospheric structure of the Tibet region (Deng et al., 2014).

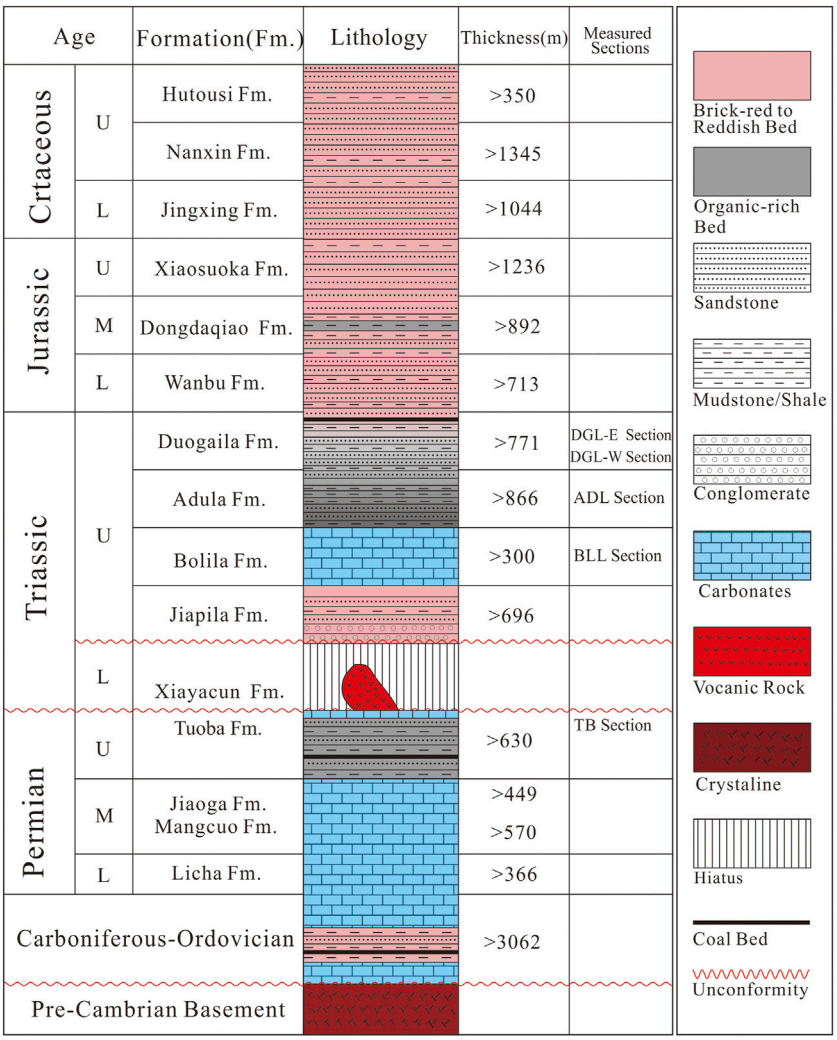


**FIGURE 3 |** Stratigraphic column and regional stratigraphic nomenclature for the Qamdo Basin (based on Tibet BGMR [Tibet Bureau of Geology and Mineral Resources], 2007).

Late Cenozoic to Recent deformation across the SE portion of the Tibet Plateau is localized on a series of strike-slip faults which accommodate the clockwise rotation of the SE Tibetan Plateau around the Eastern Himalayan Syntaxis (Burchfiel et al., 1995; Hoke et al., 2014).

The Qamdo Basin has therefore had a complex structural history since the Palaeozoic. At present the basin is bounded by the Lancangjiang Fault to the west/SW and the Zixia-Deqing Fault to the east/NE (**Figure 2**). The surface geology of the basin is characterized by widespread Upper Triassic to Cretaceous sedimentary and volcanogenic strata with local exposures of Palaeozoic to Lower Triassic sedimentary and metasedimentary rocks (**Figure 2**).

The sedimentary succession is over 12,000 m thick and the local stratigraphic nomenclature is summarised in **Figure 3** according to geological report (Tibet BGMR [Tibet Bureau of Geology and Mineral Resources], 2007). The cover succession above Precambrian basement begins with Ordovician to Permian units dominated by marine carbonates with deltaic sandstones, mudstones and coal seams. The Upper Permian Tuoba Formation includes organic-rich shales, coals and sandstones, as well as minor bioclastic limestones at the top of the unit.

Above a stratigraphic hiatus, a thick Upper Triassic to Cretaceous section occurs throughout the basin (**Figure 3**). The lower Upper Triassic Jiapila Formation includes coarse-grained alluvial, fluvial, lacustrine (evaporite), and marine (shale) deposits. Platform carbonates in the overlying middle Upper Triassic Bolila Formation are overlain by the Upper Triassic Adula and Duogaila Formations which comprise organic-rich shales, sandstones and coals deposited in a marginal marine to deltaic setting. A prominent change in colour marks the boundary between the Duogala Formation and the overlying Lower Jurassic Wangbu Formation which is composed of red-coloured sandstones. Jurassic-Cretaceous deposits are exposed in the SW of the basin between the Qamdo and Mangkang

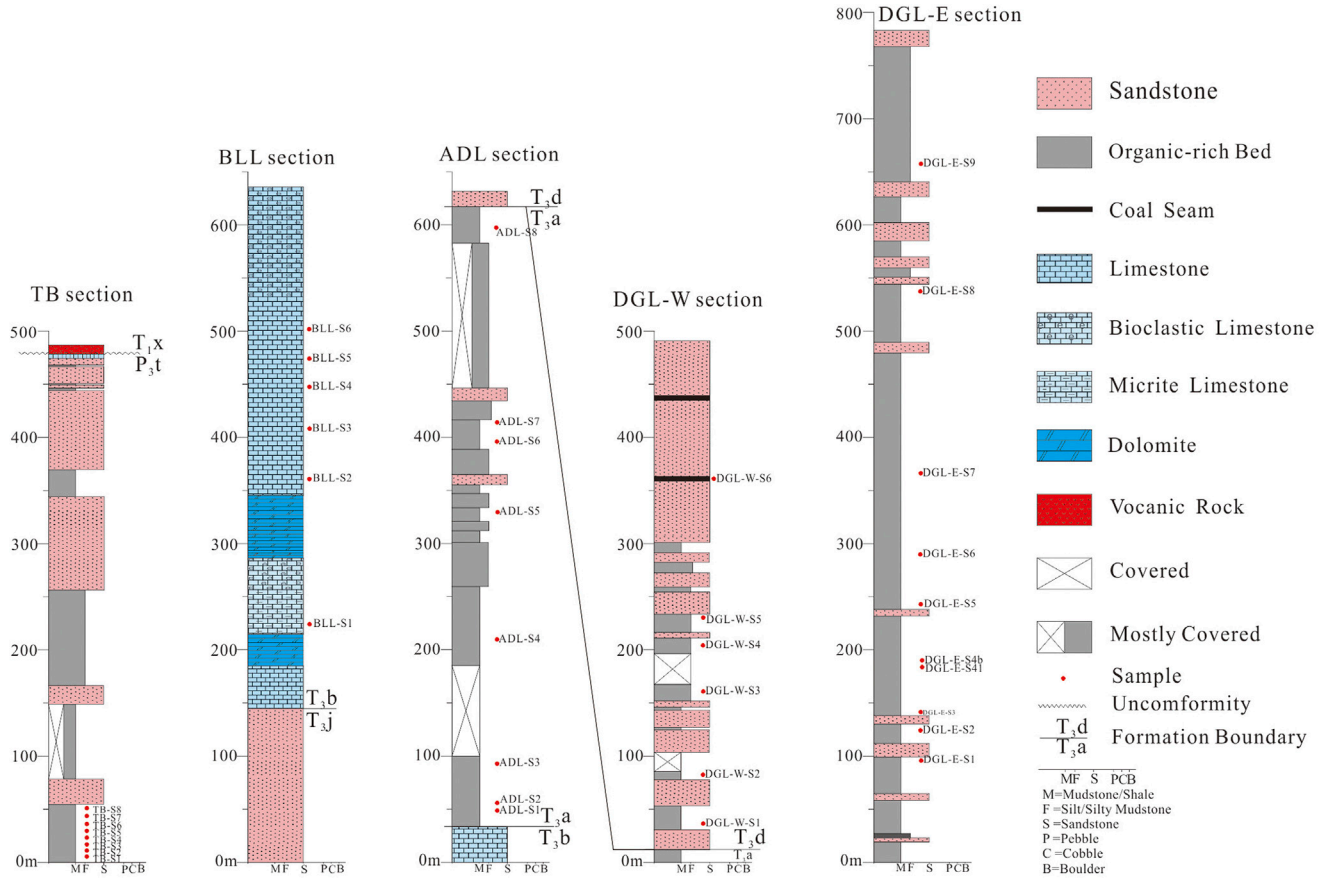


**FIGURE 4 |** Stratigraphic columns for the measured sections in the Qamdo Basin showing the locations of the studied samples. Abbreviations: P3t, Upper Permian Tuoba Formation; T1x, Lower Triassic Xiayacun Formation; T3j, Upper Triassic Jiapila Formation; T3b, Upper Triassic Bolila Formation; T3a, Upper Triassic Adula Formation; T3d, Upper Triassic Duogaila Formation.

(**Figure 1B**) and are mainly composed of fluvial-lacustrine siliciclastics; the Middle Jurassic Dongdaqiao Formation is composed of transgressive black shales (**Figure 3**).

## MATERIALS AND METHODS

### Materials

This study focuses on organic-rich shale strata in four formations in the Qamdo Basin and aims to evaluate their hydrocarbon potential. Stratigraphic sections were chosen on the basis of stratigraphic data, accessibility via roads and well-exposed conditions. Five stratigraphic sections (TB, BLL, ADL, DGL-E and DGL-W: **Figure 2**) were measured at outcrops alone the established roads.

At the TB section, about 489 m of the upper part of the Upper Permian Tuoba Formation is exposed, which is composed here of organic-rich shales, fine quartzose sandstones and bioclastic limestones (**Figures 4**, **5A**). Palaeofusulina was found in the limestones, indicating that the formation is of Changhsingian (latest Permian) age (Sheng and Wang, 1981). The cumulative thickness of dark shale on the section is over120m, which is the potential source rock of this group. Eight source rock samples were collected within a 45 m thick organic-rich shale interval in the lowermost part of the measured section (**Figure 3**).

At the BLL outcrop section, the Upper Triassic Bolila Formation is > 480 m thick and mainly consists of limestones, dolomites and bioclastic limestones. Six dark limestone samples were collected for further analysis from the upper part of the formation (**Figure 4**). The carbonates consisted of fine-grained micrite and coarse sparry calcite in the pore spaces between grains and in larger cavity structures.

The ADL section spans the entire Upper Triassic Adula Formation with a thickness of approximately 635 m and the cumulative thickness of black shale over 290 m (**Figures 4**, **5B**). The stratigraphically overlying DGL-W section (**Figures 4**, **5C**) is dominated by Upper Truiassic Duogala Formation sandstones and shales with thin coal intervals, suggesting that facies pass from prodelta to delta-plain deposits corresponding to a drop of sea level. A total of 14 samples were collection from these two sections. Another outcrop section (**Figure 5D**) of the Duogala Formation was measured to the SE (the DGL-E section) where eight samples were collected.

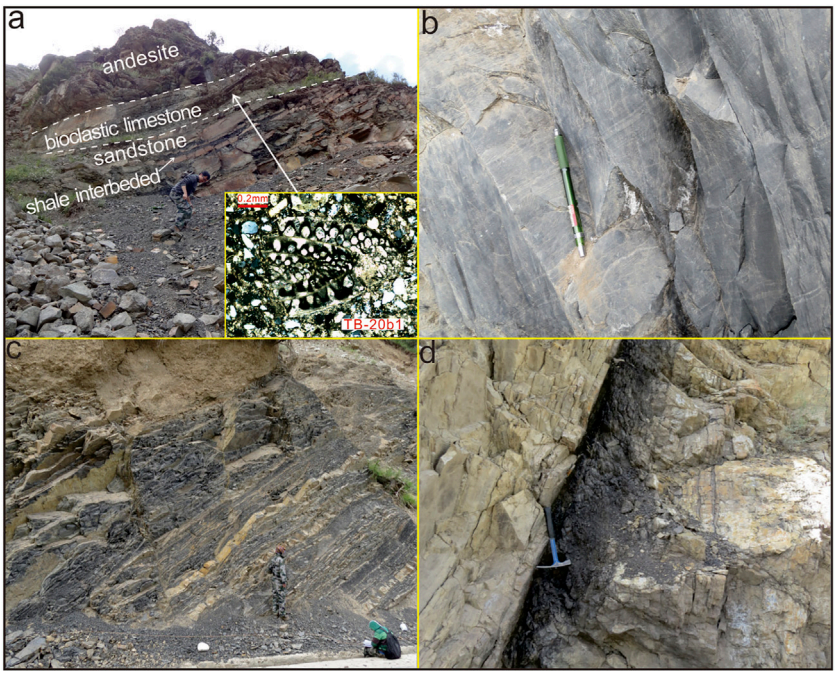


**FIGURE 5 |** Outcrop photographs showing: **(A)** brown sandstones, black shales and bioclastic limestones in the upper part of the Tuoba Formation; inset shows a fusulinid found in the limestone interval. **(B)** Dark grey mudstones of the Adula Formation; a pen (15 cm) for scale. **(C)** Black mudstones and sandstones of the Duogaila Formation outcropping at the DGL-W section. **(D)** Coal seam in the upper part of the DGL-W section; a hammer (30 cm) for scale.

## Methods

For laboratory investigations, the samples were cleaned and weathered surfaces were removed. They were ground to analytical grain sizes (approximately 100 mg and 120 μm) and dried prior to further treatment. After the removal of carbonates using hydrochloric acid (HCl), a Leco CS-200 carbon–sulphur elemental analyzer was used to determine the total organic carbon (TOC) and total sulphur (TS) contents. The samples were also analysed by a Rock–Eval II instrument following the guidelines of Peters (1986).

A total of 29 samples were selected for further analysis as they contained abundant organic matter. The crushed samples were extracted with chloroform in a Soxhlet apparatus for 72 h. The extracted organic matter was further separated by a silica gel alumina column chromatography into saturated hydrocarbons, aromatic hydrocarbons and NSO (nitrogen, sulfur, and oxygen bearing compounds) compounds (Petersen et al., 2005). The saturated hydrocarbon fractions in the extracts were analysed by gas chromatography using an Agilent 6890N (GC) instrument with an injector temperature of 310°C. The GC was equipped with a 30 m × 0.20 mm internal diameter fused silica column (0.2 μm film) using helium as the carrier gas. The oven was gradually heated from 70 to 300°C at a rate of 8°C/min and followed by an isothermal period of 20 min.

To prepare kerogen material, carbonates were first removed using HCl. Then samples were washed several times with distilled water and treated with hydrofluoric acid (HF) for 12 h to remove silicates; this step was repeated until pure kerogens were isolated (c.f. Guthrie and Pratt, 1994; Ma et al., 2015). Strew-mounted kerogen slides were then prepared and used for further identification. A visual estimation of the relative abundance of macerals was conducted using an Axioskop2 plus microscope and a Swift point counter. To determine the relative abundance of macerals, at least 300 components were counted (Petersen et al., 2005). The vitrinite reflectance (% Ro) was determined using a MPM-80 microphotometer.

Elemental analyses were performed on a FLASH EA-1112 Series elemental analyzer according to National Standard of P.R. China (GB/T 19,143–2003).

Experimental work was performed at the Organic Geochemistry Laboratory, Institute of Exploration and Development, Huabei Oilfield Branch Company of the China National Petroleum Corporation (CNPC).

## RESULTS

### Total Organic Carbon and Rock-Eval

TOC, TS and Rock-eval data of the outcrop samples from the measured sections are presented in **Table 1**. The TOC content of the eight Tuoba Formation samples from the TB section varies between 1.66 wt% and 3.01 wt%, with an average of 2.33 wt%. The S1 and S2 values are in the range of 0.–0.22 mg HC/g rock and 0.29–4.29 mg HC/g rock, respectively. Low TOCs (<0.30 wt%) were recorded in the Bolila Formation limestone samples from the BLL section, and the Adula Formation samples (ADL section) also have relatively low TOC (0.43–0.75% wt%). The samples of

**TABLE 1 |** The results of TOC, TS, Roc-eval data, vitrinite reflectance (%$R_o$) and maceral compositon (vol%) of the kerogen.

| Samples No | Lithology | TOC (wt%) | TS (wt%) | Rock-eval data (mgHC/g) | | | | | %$R_o$(n) | Maceral Compositon (vol%) | | |
|---|---|---|---|---|---|---|---|---|---|---|---|---|
| | | | | $S_0$ | $S_1$ | $S_2$ | $T_{max}$ | PY($S_1$+$S_2$) | | AOM | Vitrinite (%) | Inertinite (%) |
| ***TB section*** | | | | | | | | | | | | |
| TB-S1 | Shale | 3.01 | 0.83 | 0.03 | 0.14 | 0.42 | 522 | 0.56 | 1.96 (32) | 48 | 38 | 14 |
| TB-S2 | Shale | 2.83 | 0.89 | 0.02 | 0.24 | 0.40 | 505 | 0.63 | 1.96 (29) | 47 | 38 | 15 |
| TB-S3 | Shale | 1.71 | 0.86 | 0.01 | 0.05 | 0.22 | 522 | 0.26 | 1.95 (20) | 48 | 30 | 22 |
| TB-S4 | Shale | 2.00 | 0.95 | 0.02 | 0.21 | 0.31 | 522 | 0.52 | 1.96 (30) | 49 | 21 | 30 |
| TB-S5 | Shale | 1.66 | 0.94 | 0.02 | 0.08 | 0.31 | 522 | 0.39 | 1.96 (23) | 52 | 20 | 28 |
| TB-S6 | Shale | 1.96 | 1.12 | 0.02 | 0.10 | 0.26 | 522 | 0.36 | 1.95 (33) | 53 | 20 | 27 |
| TB-S7 | Shale | 2.59 | 1.06 | 0.02 | 0.06 | 0.30 | 522 | 0.36 | 1.94 (32) | 49 | 24 | 27 |
| TB-S8 | Shale | 2.88 | 0.60 | 0.02 | 0.08 | 0.30 | 522 | 0.38 | 1.97 (36) | 51 | 25 | 24 |
| ***BLL section*** | | | | | | | | | | | | |
| BLL-S1 | Limestone | 0.04 | 0.01 | \ | \ | \ | \ | \ | \ | \ | \ | \ |
| BLL-S2 | Limestone | 0.30 | 0.50 | \ | \ | \ | \ | \ | \ | \ | \ | \ |
| BLL-S3 | Limestone | 0.05 | 0.01 | \ | \ | \ | \ | \ | \ | \ | \ | \ |
| BLL-S4 | Limestone | 0.05 | 0.02 | \ | \ | \ | \ | \ | \ | \ | \ | \ |
| BLL-S5 | Limestone | 0.10 | 0.12 | \ | \ | \ | \ | \ | \ | \ | \ | \ |
| BLL-S6 | Limestone | 0.04 | 0.02 | \ | \ | \ | \ | \ | \ | \ | \ | \ |
| ***ADL section*** | | | | | | | | | | | | |
| ADL-S1 | Mudstone | 0.69 | 0.13 | 0.01 | 0.03 | 0.10 | 522 | 0.13 | 2.02 (17) | 67 | 3 | 30 |
| ADL-S2 | Mudstone | 0.59 | 0.13 | 0.02 | 0.05 | 0.09 | 538 | 0.14 | 2.46 (15) | 66 | 3 | 31 |
| ADL-S3 | Mudstone | 0.58 | 0.13 | 0.01 | 0.02 | 0.09 | 507 | 0.11 | 2.35 (19) | 67 | 2 | 31 |
| ADL-S4 | Mudstone | 0.59 | 0.13 | 0.01 | 0.09 | 0.14 | 469 | 0.23 | 2.46 (11) | 68 | 4 | 28 |
| ADL-S5 | Mudstone | 0.75 | 0.28 | 0.01 | 0.02 | 0.09 | 522 | 0.11 | 2.45 (13) | 65 | 4 | 31 |
| ADL-S6 | Mudstone | 0.43 | 0.10 | \ | \ | \ | \ | | \ | \ | \ | \ |
| ADL-S7 | Mudstone | 0.47 | 0.11 | \ | \ | \ | \ | | \ | \ | \ | \ |
| ADL-S8 | Mudstone | 0.62 | 0.31 | 0.01 | 0.03 | 0.12 | 522 | 0.15 | 2.47 (13) | 69 | 2 | 29 |
| ***DGL-W section*** | | | | | | | | | | | | |
| DGL-W-S1 | Mudstone | 0.64 | 0.26 | 0.01 | 0.04 | 0.10 | 522 | 0.14 | 2.40 (17) | 68 | Trace | 32 |
| DGL-W-S2 | Mudstone | 0.48 | 0.33 | 0.01 | 0.04 | 0.39 | 424 | 0.43 | 2.51 (13) | 66 | 3 | 31 |
| DGL-W-S3 | Mudstone | 0.87 | 0.30 | 0.01 | 0.06 | 0.38 | 439 | 0.44 | 2.47 (22) | 65 | 4 | 31 |
| DGL-W-S4 | Mudstone | 0.77 | 0.38 | 0.02 | 0.15 | 0.18 | 522 | 0.33 | 2.38 (25) | 67 | 5 | 28 |
| DGL-W-S5 | Mudstone | 3.47 | 0.33 | 0.01 | 0.03 | 0.23 | 522 | 0.26 | 2.29 (29) | 32 | 30 | 38 |
| DGL-W-S6 | Coal | 25.60 | 0.40 | 0.02 | 0.23 | 0.78 | 522 | 1.01 | 2.32 (32) | 46 | 18 | 34 |
| ***DGL-E section*** | | | | | | | | | | | | |
| DGL-E-S1 | Mudstone | 0.55 | 0.11 | 0.01 | 0.03 | 0.21 | 448 | 0.24 | 2.13 (17) | 60 | 15 | 25 |
| DGL-E-S2 | Mudstone | 0.63 | 0.10 | 0.01 | 0.03 | 0.39 | 437 | 0.41 | 2.00 (21) | 58 | 19 | 23 |
| DGL-E-S3 | Mudstone | 0.59 | 0.26 | 0.01 | 0.02 | 0.27 | 446 | 0.28 | 1.54 (27) | 45 | 25 | 30 |
| DGL-E-S4a | Mudstone | 0.69 | 0.10 | 0.01 | 0.02 | 0.30 | 435 | 0.32 | 1.60 (22) | 40 | 35 | 25 |
| DGL-E-S4b | Mudstone | 1.04 | 0.21 | 0.01 | 0.03 | 0.44 | 442 | 0.47 | 1.61 (18) | 64 | 19 | 17 |
| DGL-E-S5 | Mudstone | 0.66 | 0.12 | 0.01 | 0.03 | 0.38 | 435 | 0.42 | 1.63 (23) | 55 | 20 | 25 |
| DGL-E-S6 | Mudstone | 0.93 | 0.13 | 0.01 | 0.03 | 0.18 | 522 | 0.21 | 1.67 (12) | 46 | 30 | 24 |
| DGL-E-S7 | Mudstone | 0.81 | 0.11 | 0.01 | 0.03 | 0.35 | 427 | 0.38 | 1.60 (18) | 58 | 20 | 22 |
| DGL-E-S8 | Mudstone | 0.61 | 0.10 | 0.02 | 0.07 | 0.38 | 431 | 0.45 | 1.63 (30) | 57 | 23 | 20 |
| DGL-E-S9 | Mudstone | 0.47 | 0.11 | \ | \ | \ | \ | \ | \ | \ | \ | \ |

*TOC, total organic carbon; TS, total sulphur; S1, free hydrocarbons emitted from rock without cracking of kerogen; S2, residual hydrocarbons representing the remaining generative hydrocarbon potential; Tmax, Temperature reached during maximum generation of hydrocarbons measured via S2 peak of Rock-Eval pyrolysis; PY, Potential yield (=S1+S2); $R_o$ (n), Vitrinite reflectance (n: points measured); AOM, amorphous organic matter; \, No data.*

the Duogaila Formation from the DGL-W section have TOC contents ranging from 0.48 to 3.47 wt%, with the exception of the coaly samples DGL-W-S6 (TOC = 25.60 wt%). In the DGL-E section, the TOC contents of the Duogaila Formation samples are 0.47–1.04 wt% (average: 0.70 wt%).

The average S1, S2, potential yield (PY) values are 0.12, 0.32 and 0.44 mgHC/g rock for samples from the Tuoba Formation, 0.04, 0.11 and 0.15 mgHC/g rock for samples from the Adula Formation, and 0.06, 0.33, and 0.39 mgHC/g rock for samples from the Duogaila Formation, respectively (**Table 1**). The $T_{max}$ values fall within the range of 424–538°C and an average of 492°C.

## Maceral Composition and Vitrinite Reflectance

The maceral composition (vol%) and vitrinite reflectance (Ro) values for selected samples from the Tuoba, Adula and Duogaila Formations are shown in **Table 1**. About 47–53 vol% of the total organic matter (OM) in the Tuoba Formation samples from the TB section is composed of amorphous organic matter (AOM). Vitrinite and inertinite account for about 20–38 vol% and 14–30 vol% of the kerogen assemblages, respectively (**Figure 6A**).

In Adula Formation samples from the ADL section, AOM dominates the maceral composition with proportions of

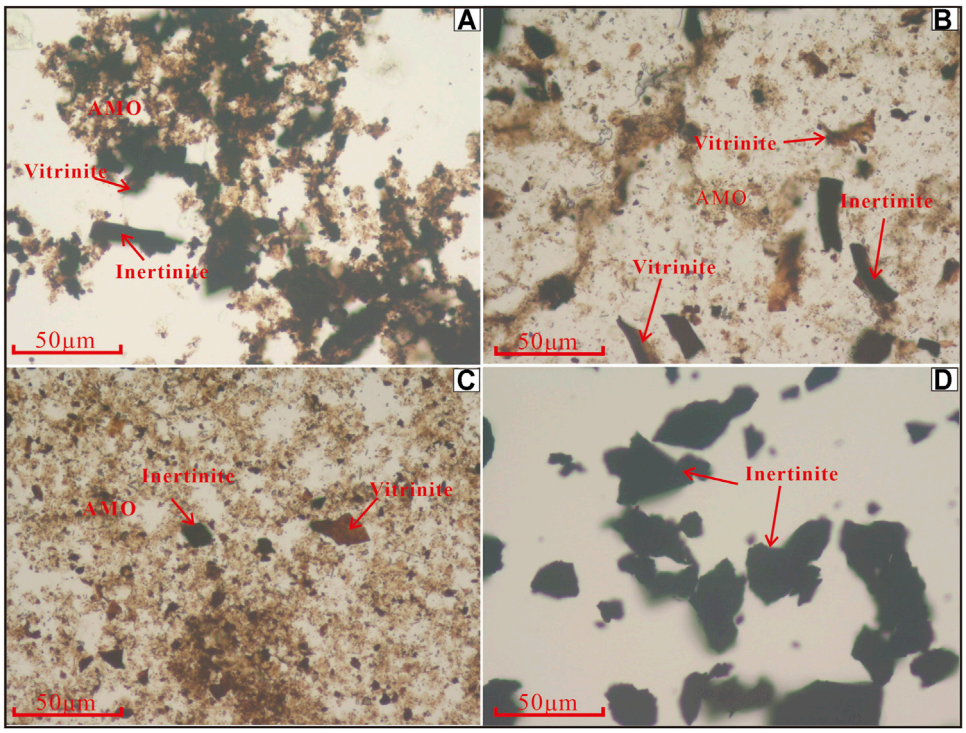


**FIGURE 6 |** Photomicrographs (intransmitted light) of macerals in samples from the Tuoba and Duogaila Formations (AMO: amorphous organic matter) **(A)** Photomicrograph showing dominant AMO together with minor inertinite (sample No. TB-S2: Tuoba Formation); **(B)** Photomicrograph showing dominant AMO relative to inertinite and vitrinite (sample No. DGL-E-S7: Duogaila Formation). **(C)** Photomicrograph showing abundant AMO compared to inertinite and vitrinite (sample No. DGL-E-S9: Duogaila Formation). **(D)** Photomicrograph showing mostly inertinite (coal sample from DGL-W section: Duogaila Formation).

more than 65 vol% of total OM. Inertinite group macerals accounts for 28%-31 vol% of the kerogen, and vitrinite up to 4 vol%.

In the DGL-E section samples, AOM is present as 40–64 vol%, whereas vitrinite and inertinite range from 15 to 35 vol% and 17 to 30 vol%, respectively (**Figures 6B,C**).

Within the eight Duogaila Formation samples from the DGL-W location, the samples from lower part of the section are dominated by AOM (65–68 vol%), followed by 28–32 vol% inertinite and 0–5 vol% vitrinite. Samples DGL-W-S5 and DGL-W-S6 have a different maceral composition which is dominated by inertinite and vitrinite. Coal seam occurs in the upper part of the DGL-W section and the photomicrograph showing an inertinite dominated composition (**Figure 6D**).

Vitrinite reflectance (Ro) values for samples from the four measured sections are listed in **Table 1**, including the number of points measured for each sample. All of the samples have Ro values > 1.3%, and some have $R_o$ > 2.0%.

## Elemental Analysis and Gas Chromatography

Elemental analysis provides a measure of the bulk chemical properties of isolated kerogen (Katz, 1988; Wang et al., 2011b) and data are summarized in **Table 2**. In general proportions of major elements are similar in all samples. Atomic O/C ratios and H/C ratios range from 0.05 to 0.16 and 0.48 to 1.38, respectively (**Table 2**).

Gas chromatograms of saturated hydrocarbon fractions in extracts of the samples are shown in **Figure 7**, and calculated parameters are given in **Table 2**. The chromatograms display a wide range of n-alkanes and isoprenoids between $n$-$C_{15}$ and $n$-$C_{35}$. The n-alkane distribution shows a bimodal pattern with a predominance of high molecular weight compounds ($n$-$C_{23}$ -- $n$-$C_{35}$); most of the samples have a peak at $n$-$C_{25}$ or $n$-$C_{33}$. In addition, all samples show odd-over-even predominance with a moderate carbon preference index (1.09 < CPI <1.72). These results indicate a high input of terrigenous organic matter.

# DISCUSSION

## Kerogen Type and Maturity

The maceral composition can be interpreted to indicate the origin and type of kerogen. Previous studies (e.g., Hutton et al., 1994; Petersen et al., 2005; Bechtel et al., 2014; Ma et al., 2015) have suggested that alginate, liptinite, and inertinite and vitrinite can be correlated to Types I, II and III kerogens, respectively. For most of the samples, AOM derived from lipid-rich precursors accounts for the largest proportion (nearly 50 vol%) of OM relative to vitrinite and inertinite macerals, suggesting that

**TABLE 2 |** Elemental analysis results and molecular geochemical data.

| Samples No | Element content | | | H/C ratio | O/C ratio | Moleculer geochemical data | | | |
|---|---|---|---|---|---|---|---|---|---|
| | C% | H% | O% | | | Pr/Ph | Pr/$n$-$C_{17}$ | Ph/$n$-$C_{18}$ | CPI |
| *TB section* | | | | | | | | | |
| TB-S1 | 34.41 | 2.21 | 2.93 | 0.77 | 0.06 | 0.73 | 0.85 | 1.28 | 1.18 |
| TB-S2 | 31.16 | 2.44 | 3.09 | 0.94 | 0.07 | 0.77 | 0.76 | 1.23 | 1.17 |
| TB-S3 | 30.55 | 2.13 | 3.61 | 0.84 | 0.09 | 0.66 | 0.65 | 1.06 | 1.16 |
| TB-S4 | 30.86 | 2.23 | 2.84 | 0.87 | 0.07 | 0.77 | 0.94 | 1.31 | 1.18 |
| TB-S5 | 33.59 | 2.69 | 4.07 | 0.96 | 0.09 | 0.75 | 0.67 | 1.18 | 1.20 |
| TB-S6 | 33.17 | 2.56 | 4.17 | 0.93 | 0.09 | 0.67 | 0.69 | 1.09 | 1.18 |
| TB-S7 | 36.51 | 2.92 | 4.28 | 0.96 | 0.09 | 0.85 | 0.84 | 1.14 | 1.18 |
| TB-S8 | 34.54 | 2.67 | 4.09 | 0.93 | 0.09 | 0.82 | 0.94 | 1.34 | 1.20 |
| *ADL section* | | | | | | | | | |
| ADL-S1 | 42.45 | 2.31 | 2.74 | 0.65 | 0.05 | 0.72 | 0.89 | 1.28 | 1.21 |
| ADL-S2 | 34.22 | 2.72 | 2.73 | 0.95 | 0.06 | 0.71 | 0.73 | 1.14 | 1.18 |
| ADL-S3 | 39.53 | 3.28 | 3.27 | 0.99 | 0.06 | 0.77 | 0.81 | 1.17 | 1.19 |
| ADL-S4 | 32.29 | 2.53 | 3.65 | 0.94 | 0.08 | 0.65 | 0.71 | 1.45 | 1.40 |
| ADL-S5 | 34.78 | 2.79 | 3.22 | 0.96 | 0.07 | 0.70 | 0.82 | 1.34 | 1.25 |
| ADL-S8 | 34.24 | 2.23 | 2.16 | 0.78 | 0.05 | 0.81 | 0.89 | 1.13 | 1.72 |
| *DGL-W section* | | | | | | | | | |
| DGL-W-S1 | 32.32 | 3.39 | 2.46 | 1.26 | 0.06 | 0.66 | 0.83 | 1.03 | 1.17 |
| DGL-W-S2 | 33.66 | 3.67 | 3.31 | 1.31 | 0.07 | 0.57 | 0.70 | 1.32 | 1.28 |
| DGL-W-S3 | 31.46 | 3.48 | 4.96 | 1.33 | 0.12 | 0.44 | 0.85 | 2.54 | 1.32 |
| DGL-W-S4 | 30.47 | 3.51 | 5.37 | 1.38 | 0.13 | 0.71 | 0.87 | 1.43 | 1.15 |
| DGL-W-S5 | 38.03 | 2.04 | 7.10 | 0.65 | 0.14 | 0.66 | 0.82 | 1.32 | 1.12 |
| DGL-W-S6 | 77.16 | 3.11 | 6.97 | 0.48 | 0.07 | 0.53 | 0.88 | 2.13 | 1.18 |
| *DGL-E section* | | | | | | | | | |
| DGL-E-S1 | 30.11 | 2.87 | 2.94 | 1.15 | 0.07 | 0.60 | 0.83 | 1.14 | 1.14 |
| DGL-E-S2 | 32.47 | 3.19 | 2.14 | 1.18 | 0.05 | 0.60 | 0.80 | 1.29 | 1.26 |
| DGL-E-S3 | 35.04 | 3.22 | 2.24 | 1.10 | 0.05 | 0.73 | 0.75 | 1.20 | 1.33 |
| DGL-E-S4a | 30.52 | 3.01 | 3.39 | 1.18 | 0.08 | 0.63 | 0.94 | 1.99 | 1.33 |
| DGL-E-S4b | 33.68 | 3.18 | 6.58 | 1.13 | 0.15 | 0.72 | 0.84 | 1.29 | 1.13 |
| DGL-E-S5 | 33.94 | 3.26 | 6.93 | 1.15 | 0.15 | 0.84 | 0.75 | 1.07 | 1.13 |
| DGL-E-S6 | 34.20 | 3.38 | 5.06 | 1.19 | 0.11 | 0.56 | 0.64 | 0.61 | 1.09 |
| DGL-E-S7 | 31.85 | 3.31 | 6.80 | 1.25 | 0.16 | 0.73 | 0.74 | 0.58 | 1.14 |
| DGL-E-S8 | 32.54 | 3.29 | 4.64 | 1.21 | 0.11 | 0.55 | 0.85 | 1.78 | 1.14 |

*Pr, Pristine; Ph, Phytane; CPI, Carbon preference index = [($C_{25}$ + $C_{27}$ + $C_{29}$ + $C_{31}$ + $C_{33}$)/($C_{26}$ + $C_{28}$ + $C_{30}$ + $C_{32}$ + $C_{34}$) + ($C_{25}$ + $C_{27}$ + $C_{29}$ + $C_{31}$ + $C_{33}$)/($C_{24}$ + $C_{26}$ + $C_{28}$ + $C_{30}$ + $C_{32}$)]/2.*

samples from all of the measured sections contain mostly Type II kerogen with smaller proportions of Type III kerogen. A cross-plot (**Figure 8**) shows that the organic matter in the samples is mainly Type II with the exceptions of two Duogaila Formation samples from the DGL-W section which contain Type III OM. The results are consistent with the relative proportions of the maceral groups.

Vitrinite reflectance ($R_o$) is the most reliable parameter for measuring the thermal maturity of sedimentary organic matter (Tissot and Welte, 1978; Grassmann et al., 2005; Opera et al., 2013). In general, Ro values of 1.3 and 2.0% are accepted as the threshold values for highly mature and over-mature Type II kerogen (Killops and Killops, 2005). Therefore, the thermal maturity of the measured samples is high-to overmature (i.e., wet gas to dry gas zone). The results are consistent with the high $T_{max}$ value.

## Hydrocarbon Potential

Overall, the samples collected from Tuoba Formation exhibit the best hydrocarbon potential of the formations investigated with TOC >1.0 wt%. By contrast, the samples from the BLL section have TOC <0.3 wt%. Samples from the Adula and Duogala Formations have poor to medium organic contents, with the exception of a few coaly samples of the latter formation from the DGL-W section. PY (PY = S1 + S2) represents the potential yield and a quantity of the transformation potential of the total organic matter (Demaison and Huizinga, 1991; Tissot and Welte, 1978). According to evaluation criterion of the hydrocarbon source rock established by the China National Petroleum Corporation (Wang et al., 2009; Ding et al., 2013), PI value over 0.25 is classified as good source rock, and 0.15 to 0.25 for medium source rock.

The proneness towards oil or gas generation is indicated by the kerogen type and the maceral composition. Fluorescent macerals

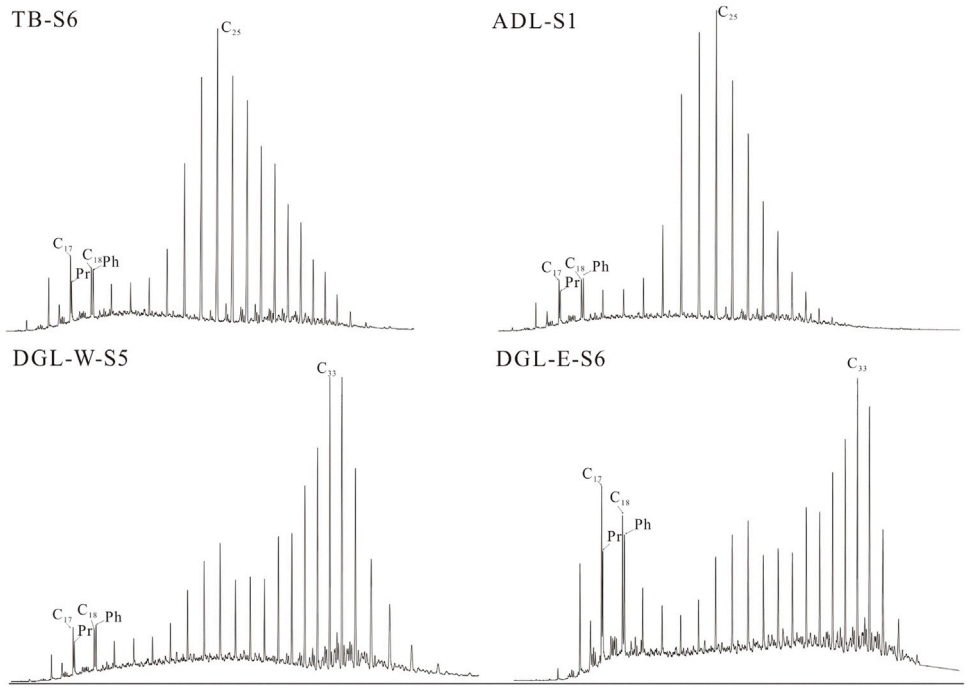


**FIGURE 7 |** Gas chromatograms of the saturated fractions for extracts from four samples (sample No. TB-S6, ADL-S1, DGL-W-S5, DGL-E-S6) showing the distribution of the n-alkanes and isoprenoids.

of the liptinite group are here considered as the oil-prone fraction, and the sum of inertinite and vitrinite group macerals are the gas-prone fraction (Killops and Killops, 2005; Furmann et al., 2015; Hakimi and Ahmed, 2016). The analysed samples contain mainly Type II OM with nearly equal oil- and gas-prone fractions. However, all the samples are highly to over-mature in terms of $R_{o,}$ as discussed above. The maturity stage of studied samples (high to over mature) is high enough to generate and expel large amount of hydrocarbons and cracked into dry gas (Killops and Killops, 2005; Liang et al., 2017), this reveals that the measured strata were underwent deep burial after deposition. Therefore, the combined evidence suggests that gas generation can be expected in the Tuoba, Adula and Duogaila Formations.

## Controls on Source Rocks Deposition

Total sulphur is considered to be a good measure of the degree of marine influence (Sykes, 2004; Sykes et al., 2014; Sarki Yandoka et al., 2015). In samples from the Tuoba Formation, TS contents varied between 0.60 and 1.12 wt%; values for samples from the ADL, DGL-W and DGL-E sections (Adula and Duogaila Formations) were much lower (0.10–0.40 wt%). Thus, compared to the Tuoba Formation, the samples from the Adula and Duogaila Formations are interpreted to have been deposited under more freshwater-influenced conditions which consistent with delta facies.

Pristane (Pr) and phytane (Ph) occur in significant amounts in all the studied samples (**Figure 7**). The most abundant source of pristane and phytane is the phytyl side-chain of chlorophyll a in phototrophic organisms, and bacterio chlorophyll a and b in purple sulphur bacteria (Powell and McKirdy, 1973). The phytyl side-chain is prone to be converted into phytane in reducing or anoxic conditions, whereas oxic conditions favour pristane (Peters et al., 2005). Therefore, the value of the Pr/Ph ratio is considered to indicate the redox conditions during sedimentation and diagenesis (Didyk, 1978; Chandra et al., 1994; Escobar et al., 2011). High Pr/Ph (>3.0) indicates oxic conditions often associated with terrigenous organic matter input, while low values (<0.8) typify anoxic, commonly hypersaline or carbonate environments (Peters et al., 2005; El Diasty and Moldowan, 2012). Phytane occurs in high relative concentrations in the analyzed samples, resulting in Pr/Ph ratios in the range of 0.44–0.85 (**Table 2**), indicating a suboxic to relatively anoxic depositional setting. Furthermore, Pr/$n$-$C_{17}$ and Ph/$n$-$C_{18}$ ratios are in the range of 0.64–0.94 and 0.58–2.54, respectively. A cross-plot of Pr/$n$-$C_{17}$ versus Ph/$n$-$C_{18}$ (**Figure 9**) also suggests that marine-derived organic matter was an important input to the source rock and was preserved under a reducing environment.

The Qamdo Basin experienced frequent sea-level fluctuations, especially in the Late Triassic, and four transgressive-regressive cycles have been recognized according to the sedimentary record (Du et al., 1997; Du et al., 1998). Based on sequence stratigraphy analyses for the outcrops in the Qamdo area, Peng et al. (2005) constructed a curve of sea level change for the Late Triassic (**Figure 10**). Compared with the eustatic cycle of Haq et al. (1988), the curve in the Qamdo area contains more low-amplitude signals relating to short-term sea-level change. **Figure 10** shows that the source rock intervals in the Adula

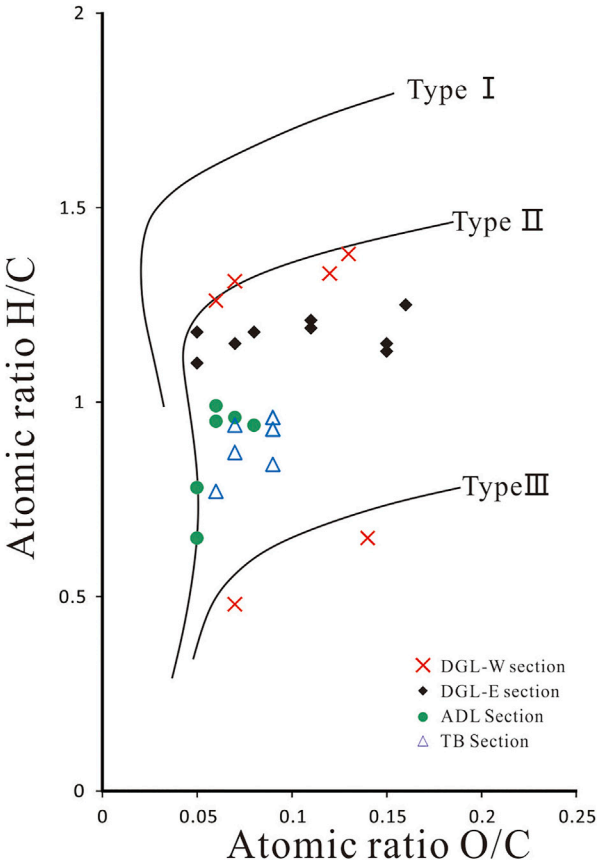


**FIGURE 8 |** Cross-plot of H/C versus O/C ratios for the analysed samples.

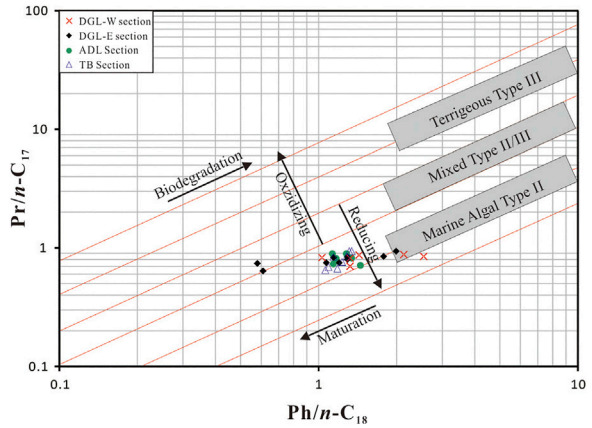


**FIGURE 9 |** Cross-plot of phytane/*n*-$C_{18}$ alkane (Ph/*n*-$C_{18}$) versus pristane/*n*-$C_{17}$ alkane (Pr/*n*-$C_{17}$) for analysed samples howing depositional conditions and source of organic matter (after Hunt, 1995; Riboulleau et al., 2007; El Diasty and Moldowan, 2012).

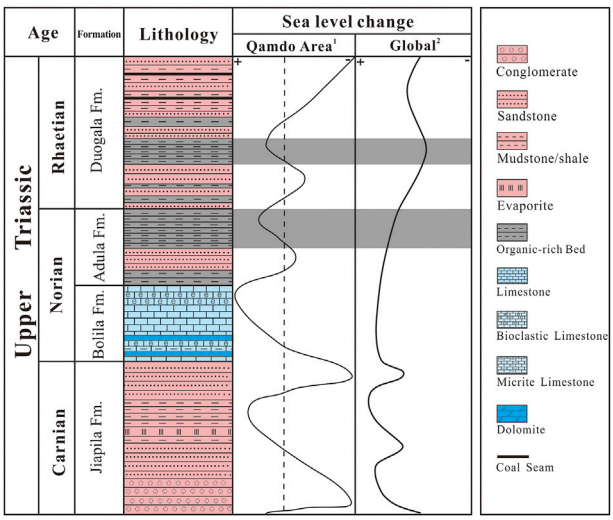


**FIGURE 10 |** Upper Triassic lithology of the Qamdo Basin and sea level curve showing that two source rock intervals correspond to transgressive episodes. Sea-level curve based on 1 Peng et al., 2005 and 2 Haq et al., 1988.

and Duogala Formations were deposited during transgressive episodes. Instead, peat deposits (coal beds of Duogaila Formation) and coarse-grained clastic deposits may be preserved in response to relative sea-level fluctuations (Diessel, 1992; Lv and Chen, 2014).

Various reasons have been proposed to account for the positive association between transgressions and the deposition of organic-rich facies (Klemme and Ulmishek, 1991; Arthur and Sageman, 1994; Arthur, 2005). including: 1) transgressive periods may enhance seasonal or longer-term water-column stratification and development of anoxia; 2) rising sea levels may promotes near-shore trapping of terrigenous clastic material, creating condensed intervals which are characterized by enrichment in organic carbon (Arthur, 2005); and 3) land-derived nutrients give rise to surface plankton booms, resulting in high biological productivity (Hao et al., 2011; Li et al., 2016).

The transgressive episodes in the Jiapila and Bilila Formations have quite different sedimentary characteristics. During Jiapila Formation deposition, intense tectonism resulted in widespread conglomerates which are have little source rock potential (Du et al., 1997; Du et al., 1998). In addition, evidence for an arid palaeoclimate in the Qamdo basin area is provided by evaporitic lacustrine deposits (Du et al., 1997; Du et al., 1998). By contrast, the Bolila Formation is characterised by the development thick platform carbonates during a period of tectonic and volcanic quiescence, during which terrigenous input was greatly reduced (Peng et al., 2005). Consequently, the accumulation of organic matter just depended on the productivity of the ocean with the insufficient nutrients.

Clearly, the development of source rock is governed by a variety of factors, such as a warm and moist climate, profitable regional tectonics and eustasy. Among them, sea level fluctuations have important implications for organic productivity of the oceans and sediment distribution patterns for the Qamdo Basin. The rise of sea level usually results in a

reduced environment, and indicators of redox (such as Pr/Ph ratio) in accord with these samples were deposited in an anoxic and reducing environment.

## CONCLUSION

Sedimentary characteristic and organic properties of Tuoba, Bolila, Adula and Duogala Formations were analysed to investigate the formations' geochemical characteristics, hydrocarbon potential, and the controls on organic matter input. The following major conclusions were reached:

1) Outcrop samples of the Tuoba Formation has relatively high TOC contents averaging 2.33%, while the Adula and Duogala Formations have poor to medium organic richness with exception of a few coaly samples from the DGL-W section. However, the Bolila Formation shows very low TOC contents lower than 0.3%, indicating that the Bolila carbonates have barely hydrocarbon generation potential.
2) Elemental analysis and maceral composition indicate that the organic matter in shale samples from the Tuoba, Adula and Duogala Formations are characterized by Type II kerogen with a mixed sources of organic matter input.
3) All of the samples analysed have high vitrinite reflectance (Ro > 1.3%) and most of the samples show a high $T_{max}$ (424–538°C). Maturity estimates based on vitrinite reflectance and Rock-eval parameters indicate that all of the samples analysed are thermally highly-to overmature.
4) According to the organic matter abundance and kerogen type evaluation for the samples of the Qamdo Basin, it seems that the Late Permian Tuoba Formation is considered to be the best candidate of effective source rock. The Late Triassic Source Rocks (Adula and Duogaila Formations) shows considerable hydrocarbon potential as well. Combined with results of maturity indicators, the analysed formations have reached thermogenic dry gas window and gas generation can be expected from the Late Permian Tuoba Formation, the Late Triassic Adula and the Late Triassic Duogaila Formations.
5) Enrichment of organic carbon in the analysed formations was probably controlled by eustatic sea level changes, regional tectonics and climatic variations. Organic-rich facies accumulated during major transgressive episodes.

## DATA AVAILABILITY STATEMENT

The original contributions presented in the study are included in the article/Supplementary Material, further inquiries can be directed to the corresponding authors.

## AUTHOR CONTRIBUTIONS

ZQ wrote the manuscript, organized the database and performed the statistical analysis. YL and CW contributed to conception and design of the study. All authors contributed to manuscript revision, read, and approved the submitted version.

## FUNDING

This research is financially supported by the Strategic Priority Research Program of Chinese Academy of Sciences (Grant Nos. XDA20070303) and the Science and Technology Department of Qinghai Province- Qinghai Natural Science Foundation (Youth Project: 2019-ZJ-964Q).

## ACKNOWLEDGMENTS

We thank Xiaohan Li, Sheng Wei, Bo Wang, Jinghua Dai, Haiyang He, Yajuan Wang and Yaoyao Duan for the fieldwork, and Shunping Ma for assistance in the laboratory.

## REFERENCES

Arthur, M. A., and Sageman, B. B. (1994). Marine Black Shales: Depositional Mechanisms and Environments of Ancient Deposits. *Annu. Rev. Earth Planet. Sci.* 22, 499–551. doi:10.1146/annurev.ea.22.050194.002435

Arthur, M. A. (2005). "Sea-level Control on Source-Rock Development: Perspectives from the Holocene Black Sea, the Mid-cretaceous Western Interior Basin of North America, and the Late Devonian Appalachian Basin," in *The Deposition of Organic Carbon-rich Sediments: Models, Mechanisms and Consequences*. Editor N. B. Harris. Tulsa, Oklahoma: Society for Sedimentary Geology, 82, 35–59.

Bechtel, A., Karayiğit, A. I., Sachsenhofer, R. F., İnaner, H., Christanis, K., and Gratzer, R. (2014). Spatial and Temporal Variability in Vegetation and Coal Facies as Reflected by Organic Petrological and Geochemical Data in the Middle Miocene Çayirhan Coal Field (Turkey). *Int. J. Coal Geology.* 134-135, 46–60. doi:10.1016/j.coal.2014.09.011

Burchfiel, B. C., Zhiliang, C., Yupinc, L., and Royden, L. H. (1995). Tectonics of the Longmen Shan and Adjacent Regions, central China. *Int. Geology. Rev.* 37, 661–735. doi:10.1080/00206819509465424

Chandra, K., Mishra, C. S., Samanta, U., Gupta, A., and Mehrotra, K. L. (1994). Correlation of Different Maturity Parameters in the Ahmedabad-Mehsana Block of the Cambay basin. *Org. Geochem.* 21, 313–321. doi:10.1016/0146-6380(94)90193-7

Chang, C.-F., Pan, Y.-S., and Sun, Y.-Y. (1989). "The Tectonic Evolution of Qinghai-Tibet Plateau: a Review," in *Tectonic Evolution of the Tethyan Region*. Editor A. C. Sengör (Netherlands: Springer), 415–476. doi:10.1007/978-94-009-2253-2_18

Chang, C., Chen, N., Coward, M. P., Deng, W., Dewey, J. F., Gansser, A., et al. (1986). Preliminary Conclusions of the Royal Society and Academic Sinica 1985 Geotraverse of Tibet. *Nature* 323, 501–507.

Chen, H., Wu, Y., Xiao, Q., and He, S. (2010). Fluid Inclusion Evidence of Paleo-Oil Reservoirs in Changdu Basin, Tibet. *Acta Geologica Sinica* 84, 1457–1469. (in Chinese with English abstract).

DeCelles, P. G., Robinson, D. M., and Zandt, G. (2002). Implications of Shortening in the Himalayan Fold-thrust belt for Uplift of the Tibetan Plateau. *Tectonics* 21, 1–25. doi:10.1029/2001tc001322

Deng, J., Wang, Q., Li, G., and Santosh, M. (2014). Cenozoic Tectono-Magmatic and Metallogenic Processes in the Sanjiang Region, Southwestern China. *Earth-Science Rev.* 138, 268–299. doi:10.1016/j.earscirev.2014.05.015

Demaison, G., and Huizinga, B. J. (1991). Genetic Classification of Petroleum Systems. *AAPG Bull.* 75, 1626–1643. doi:10.1306/0C9B29BB-1710-11D7-8645000102C1865D

Didyk, B. M., Simoneit, B. R. T., Brassell, S. C., and Eglinton, G. (1978). Organic Geochemical Indicators of Palaeoenvironmental Conditions of Sedimentation. *Nature* 272, 216–222. doi:10.1038/272216a0

Diessel, C. F. K. (1992). *Coal-Bearing Depositional System-Coal Facies and Depositional Environments: 8-Coal Formation and Sequence Stratigraphy*. New York: Springer-Verlag, 465–514.

Ding, W., Wan, H., Zhang, Y., and Han, G. (2013). Characteristics of the Middle Jurassic marine Source Rocks and Prediction of Favorable Source Rock Kitchens in the Qiangtang Basin of Tibet. *J. Asian Earth Sci.* 66, 63–72. doi:10.1016/j.jseaes.2012.12.025

Du, D., Luo, J., and Hui, L. (1998). Late Palaeozoic Sequence Stratigraphy and Sea Level Changes in the Qamdo Block. *Tethyan Geology*. 22, 72–75. (in Chinese with English abstract).

Du, D., Luo, J., and Li, X. (1997). Sedimentary Evolution and Palaeogeography of the Qamdo Block in Tibet. *Sediment. Facies Palaeogeogr.* 17, 1–16. (in Chinese with English abstract).

El Diasty, W. S., and Moldowan, J. M. (2012). Application of Biological Markers in the Recognition of the Geochemical Characteristics of Some Crude Oils from Abu Gharadig Basin, north Western Desert - Egypt. *Mar. Pet. Geology.* 35, 28–40. doi:10.1016/j.marpetgeo.2012.03.001

Escobar, M., Márquez, G., Inciarte, S., Rojas, J., Esteves, I., and Malandrino, G. (2011). The organic geochemistry of oil seeps from the Sierra de Perijá eastern foothills, Lake Maracaibo Basin, Venezuela. *Org. Geochem.* 42, 727–738. doi:10.1016/j.orggeochem.2011.06.005

Fu, X., Wang, J., Zeng, Y., Li, Z., and Wang, Z. (2009). Geochemical and Palynological Investigation of the Shengli River marine Oil Shale (China): Implications for Paleoenvironment and Paleoclimate. *Int. J. Coal Geology.* 78, 217–224. doi:10.1016/j.coal.2009.02.001

Furmann, A., Mastalerz, M., Brassell, S. C., Pedersen, P. K., Zajac, N. A., and Schimmelmann, A. (2015). Organic Matter Geochemistry and Petrography of Late Cretaceous (Cenomanian-Turonian) Organic-Rich Shales from the Belle Fourche and Second White Specks Formations, West-central Alberta, Canada. *Org. Geochem.* 85, 102–120. doi:10.1016/j.orggeochem.2015.05.002

Grassmann, S., Cramer, B., Delisle, G., Messner, J., and Winsemann, J. (2005). Geological History and Petroleum System of the Mittelplate Oil Field, Northern Germany. *Int. J. Earth Sci. (Geol Rundsch)* 94, 979–989. doi:10.1007/s00531-005-0018-x

Gu, Y., Shao, Z., Ye, D., Zhang, X., and Lu, Y. (1999). Characteristics of Source Rocks and Resource prospect in the Lunpola Basin. *Tibet. Petrol. Geology. Exp.* 21, 340–345. (in Chinese with English abstract).

Guthrie, J. M., and Pratt, L. M. (1994). Geochemical Indicators of Depositional Environment and Source Rock Potential for the Upper Ordovician Maquoketa Group, Illinois Basin. *AAPG Bull.* 78, 744–757. doi:10.1306/a25fe3a1-171b-11d7-8645000102c1865d

Hakimi, M. H., and Ahmed, A. F. (2016). Petroleum Source Rock Characterisation and Hydrocarbon Generation Modeling of the Cretaceous Sediments in the Jiza sub-basin, Eastern Yemen. *Mar. Pet. Geology.* 75, 356–373. doi:10.1016/j.marpetgeo.2016.04.008

Hao, F., Zhou, X., Zhu, Y., and Yang, Y. (2011). Lacustrine Source Rock Deposition in Response to Co-evolution of Environments and Organisms Controlled by Tectonic Subsidence and Climate, Bohai Bay Basin, China. *Org. Geochem.* 42, 323–339. doi:10.1016/j.orggeochem.2011.01.010

Haq, B. U., Hardenbol, J., and Vail, P. R. (1988). Mesozoic and Cenozoic Chronostratigraphy and Cycles of Sea-Level Change. *Spec. Publications SEPM* 42, 71–108. doi:10.2110/pec.88.01.0071

Hoke, G. D., Liu-Zeng, J., Hren, M. T., Wissink, G. K., and Garzione, C. N. (2014). Stable Isotopes Reveal High Southeast Tibetan Plateau Margin since the Paleogene. *Earth Planet. Sci. Lett.* 394, 270–278. doi:10.1016/j.epsl.2014.03.007

Huang, K., Opdyke, N. D., Li, J., and Peng, X. (1992). Paleomagnetism of Cretaceous Rocks from Eastern Qiangtang Terrane of Tibet. *J. Geophys. Res.* 97, 1789–1799. doi:10.1029/91jb02747

Hunt, J. M. (1995). *Petroleum Geochemistry and Geology*. New York: W. H. Freeman.

Hutton, A., Bharati, S., and Robl, T. (1994). Chemical and Petrographic Classification of Kerogen/macerals. *Energy Fuels* 8, 1478–1488. doi:10.1021/ef00048a038

Katz, B. J. (1988). "Clastic and Carbonate Lacustrine Systems: an Organic Geochemical Comparison (Green River Formation and East African lake Sediments)," in *Lacustrine Petroleum Source Rocks*. Editors A. J. Fleet, K. Kelts, and M. R. Talbot (Oxford: Geological Society London Special Publications), 40, 81–90. doi:10.1144/gsl.sp.1988.040.01.08

Killops, S., and Killops, V. (2005). *Introduction to Organic Geochemistry*. second ed.. Oxford: Blackwell Publishing.

Klemme, H., and Ulmishek, G. F. (1991). Effective Petroleum Source Rocks of the World: Stratigraphic Distribution and Controlling Depositional Factors. *AAPG Bull.* 75, 1809–1851. doi:10.1306/0c9b2a47-1710-11d7-8645000102c1865d

Li, W., Zhang, Z., Li, Y., and Fu, N. (2016). The Effect of River-delta System on the Formation of the Source Rocks in the Baiyun Sag, Pearl River Mouth Basin. *Mar. Pet. Geology.* 76, 279–289. doi:10.1016/j.marpetgeo.2016.05.033

Liang, C., Jiang, Z., Cao, Y., Zhang, J., and Guo, L. (2017). Sedimentary Characteristics and Paleoenvironment of Shale in the Wufeng-Longmaxi Formation, North Guizhou Province, and its Shale Gas Potential. *J. Earth Sci.* 28, 1020–1031. doi:10.1007/s12583-016-0932-x

Lv, D., and Chen, J. (2014). Depositional Environments and Sequence Stratigraphy of the Late Carboniferous–Early Permian Coal-Bearing Successions (Shandong Province, China): Sequence Development in an Epicontinental basin. *J. Asian Earth Sci.* 79, 16–30. doi:10.1016/j.jseaes.2013.09.003

Ma, P., Wang, C., Wang, L., Li, Y., and Hu, J. (2015). Sedimentology and Organic Properties of Lower Tertiary Lacustrine Source Rocks, Lunpola Basin, central Tibetan Plateau: Implications for Hydrocarbon Potential. *Mar. Pet. Geology.* 66, 1029–1041. doi:10.1016/j.marpetgeo.2015.08.013

Opera, A., Alizadeh, B., Sarafdokht, H., Janbaz, M., Fouladvand, R., and Heidarifard, M. H. (2013). Burial History Reconstruction and thermal Maturity Modeling for the Middle Cretaceous-Early Miocene Petroleum System, Southern Dezful Embayment, SW Iran. *Int. J. Coal Geology.* 120, 1–14. doi:10.1016/j.coal.2013.08.008

Pan, G., Wang, L., Li, R., Yuan, S., Ji, W., Yin, F., et al. (2012). Tectonic Evolution of the Qinghai-Tibet Plateau. *J. Asian Earth Sci.* 53, 3–14. doi:10.1016/j.jseaes.2011.12.018

Peng, Y., Liu, J., and Luo, J. (2005). *Triassic Sequence Stratigraphy and Evolution of Sedimentary basin in Qamdo Area*. Beijing: Geological Publishing House. (in Chinese with English abstract).

Peters, K. E. (1986). Guidelines for Evaluating Petroleum Source Rock Usingprogrammed Pyrolysis. *AAPG Bull.* 70, 318–329. doi:10.1306/94885688-1704-11d7-8645000102c1865d

Peters, K. E., Walter, C. C., and Moldowan, J. M. (2005). *Biomarkers and Isotopes in Petroleum Exploration and Earth History*, Vol. 2. UK: Cambridge University Press, 475–1155. The Biomarker Guide.

Petersen, H. I., Tru, V., Nielsen, L. H., Duc, N. A., and Nytoft, H. P. (2005). Source Rock Properties of Lacustrine Mudstones and Coals (Oligocene Dong Ho Formation), Onshore Song Hong Basin, Northern Vietnam. *J. Pet. Geol* 28, 19–38. doi:10.1111/j.1747-5457.2005.tb00068.x

Powell, T. G., and McKirdy, D. M. (1973). Relationship between Ratio of Pristane to Phytane, Crude Oil Composition and Geological Environment in Australia. *Nat. Phys. Sci.* 243, 37–39. doi:10.1038/physci243037a0

Riboulleau, A., Schnyder, J., Riquier, L., Lefebvre, V., Baudin, F., and Deconinck, J.-F. (2007). Environmental Change during the Early Cretaceous in the Purbeck-type Durlston Bay Section (Dorset, Southern England): A Biomarker Approach. *Org. Geochem.* 38, 1804–1823. doi:10.1016/j.orggeochem.2007.07.006

Sarki Yandoka, B. M., Abdullah, W. H., Abubakar, M. B., Hakimi, M. H., and Adegoke, A. K. (2015). Geochemistry of the Cretaceous Coals from Lamja Formation, Yola Sub-basin, Northern Benue Trough, NE Nigeria: Implications for Paleoenvironment, Paleoclimate and Tectonic Setting. *J. Afr. Earth Sci.* 104, 56–70. doi:10.1016/j.jafrearsci.2015.01.002

Sheng, J., and Wang, Y. (1981). Permian Fusulinids from Tibet (Xizang) with Reference to Their Geographical Provincialism. *Acta Palaeontologica Sinica* 20, 546–551. (in Chinese with English abstract).

Sichuan BGMR [Sichuan Bureau of Geology and Mineral Resources], 2007. *Sichuan Bureau of Geology and Mineral Resources.*

Sykes, R. (2004). Peat Biomass and Early Diagenetic Controls on the Paraffinic Oil Potential of Humic Coals, Canterbury Basin, New Zealand. *Pet. Geosci.* 10, 283–303. doi:10.1144/1354-079302-568

Sykes, R., Volk, H., George, S. C., Ahmed, M., Higgs, K. E., Johansen, P. E., et al. (2014). Marine Influence Helps Preserve the Oil Potential of Coaly Source Rocks: Eocene Mangahewa Formation, Taranaki Basin, New Zealand. *Org. Geochem.* 66, 140–163. doi:10.1016/j.orggeochem.2013.11.005

Tan, F. W., Wang, J., Wang, X. L., and Du, B. W. (2002). Discovery of the Most Extensive Asphalt Veins in the Qiangtang basin, Northern Tibet. *Reg. Geology. China* 21 (11), 801–802. (in Chinese with English abstract).

Taner, I., and Meyerhoff, A. A. (1990a). Petroleum at the Roof of the World: The Geological Evolution of the Tibet (Qinghai-Xizang) Plateau Part I. *J. Pet. Geol* 13 (2), 157–177. doi:10.1111/j.1747-5457.1990.tb00837.x

Taner, I., and Meyerhoff, A. A. (1990b). Petroleum at the Roof of the World: The Geological Evolution of the Tibet (Qinghai-Xizang) Plateau Part II. *J. Pet. Geol* 13 (3), 289–314. doi:10.1111/j.1747-5457.1990.tb00848.x

Tibet BGMR [Tibet Bureau of Geology and Mineral Resources], 2007. *Tibet Bureau of Geology and Mineral Resources*.

Tissot, B. P., and Welte, D. H. (1978). *Petroleum Formation and Occurrence*. Springer-Verlag, 699.

Wang, C., Dai, J., Zhao, X., Li, Y., Graham, S. A., He, D., et al. (2014). Outward-growth of the Tibetan Plateau during the Cenozoic: A Review. *Tectonophysics* 621, 1–43. doi:10.1016/j.tecto.2014.01.036

Wang, C., Li, Y., and Li, Y. (2006). Discussion on Evaluation of Oil and Gas Resources in Qinghai-Tibet Plateau. *Acta Petrol. Ei Sinica* 27, 1–7. (in Chinese with English abstract).

Wang, C., and Zhang, S. (1996). Preliminary Analysis of Petroliferous Basins and Oi-Lgas Prospects in Qinghai-Xizang (Tibet) Plateau. *Earth Sci.* 21, 120–129. (in Chinese with English abstract).

Wang, J., Ding, J., Wang, C. S., Tab, F. W., Chen, M., Hu, P., et al. (2009). *Survey and Evaluation on Tibet Oil and Gas Resources*. Beijing: Geological Publishing House, 215. (in Chinese).

Wang, L., Wang, C., Li, Y., Zhu, L., and Wei, Y. (2011b). Organic Geochemistry of Potential Source Rocks in the Tertiary Dingqinghu Formation, Nima basin, central Tibet. *J. Pet. Geology.* 34 (1), 67–85. doi:10.1111/j.1747-5457.2011.00494.x

Wang, L., Wang, C., Li, Y., Zhu, L., and Wei, Y. (2011a). Sedimentary and Organic Geochemical Investigation of Tertiary Lacustrine Oil Shale in the central Tibetan Plateau: Palaeolimnological and Palaeoclimatic Significances. *Int. J. Coal Geology.* 86, 254–265. doi:10.1016/j.coal.2011.02.011

Wu, Y., Chen, H., Xiao, Q., and Zhai, P. (2010). Characteristics of Flow of the Upper Triassic in Changdu Basin, Tibet, China. *Geol. Sci. Techn. Inf.* 29, 82–86. (in Chinese with English abstract).

Xu, H., Pu, X., and Han, D. (2004). Oil-bearing Characteristics Identification in Surface Sandstones: Taking Cuoqing, Kekexili, Biru and Changdu Basins in Tibet for Example. *Pet. Geology. Exp.* 26, 68–73. (in Chinese with English abstract). doi:10.1016/j.jsg.2004.06.004

Yang, R., Cao, J., Hu, G., and Fu, X. (2015). Organic Geochemistry and Petrology of Lower Cretaceous Black Shales in the Qiangtang Basin, Tibet: Implications for Hydrocarbon Potential. *Org. Geochem.* 86, 55–70. doi:10.1016/j.orggeochem.2015.06.006

Yin, A., and Harrison, T. M. (2000). Geologic Evolution of the Himalayan-Tibetan Orogen. *Annu. Rev. Earth Planet. Sci.* 28, 211–280. doi:10.1146/annurev.earth.28.1.211

Zeng, Y. H., Fu, X. G., Zeng, S. Q., and Du, G. (2013). Upper Triassic Potential Source Rocks in the Qiangtang Basin, Tibet: Organic Geochemical Characteristics. *J. Pet. Geology.* 36 (3), 237–255. doi:10.1111/jpg.12554

**Conflict of Interest:** The authors declare that the research was conducted in the absence of any commercial or financial relationships that could be construed as a potential conflict of interest.

**Publisher's Note:** All claims expressed in this article are solely those of the authors and do not necessarily represent those of their affiliated organizations, or those of the publisher, the editors and the reviewers. Any product that may be evaluated in this article, or claim that may be made by its manufacturer, is not guaranteed or endorsed by the publisher.